A solar-assisted low-temperature district heating and cooling network coupled with a ground-source heat pump

S. Bordignon[1], D. Quaggiotto[1*], J. Vivian[1,2], G. Emmi[1,3], M. De Carli[1], A. Zarrella[1]

[1]Department of Industrial Engineering – University of Padova, Padova, Italy

[2]Department of Architecture – University of Ferrara, Ferrara, Italy

[1] Department of Industrial Engineering - Applied Physics Section, University of Padova, Via Venezia 1 – 35131, Padova, Italy.

[2] Urban Energy Systems Lab - Swiss Federal Laboratories for Materials Science and Technology (EMPA), Ueberlandstrasse 129 – 8600 Dübendorf, Switzerland.

[3] Department of Architecture, University of Ferrara, Via Quartieri 8 – 44121 Ferrara, Italy

Abstract

Towards the development of highly integrated and energy efficient heating and cooling systems, with an energy community perspective, the present paper proposes a novel technical solution for the provision of air-conditioning, domestic hot water and electricity to a small residential district in heating-dominant regions. Three reference climates have been considered: Helsinki, Berlin and Strasbourg. Detailed dynamic models have been created using TRNSYS and NeMo, and long term operations of the energy system, including a new-generation ultra-low temperature district heating and cooling network have been performed. The core of the energy system is the network supplied by a high-efficiency ground source heat pump and used as the source and sink by booster heat pumps installed in the substations. Rooftop photovoltaic thermal panels partially meet the electrical demand of the district, as well as the thermal load for domestic hot water production. Moreover, the panels are cooled by the network, obtaining a reduction in the thermal unbalance to the ground and enhancing their electrical efficiency. This solution allows obtaining high coefficient of performance for the heat pumps in the substations and supply stations, reaching values of 5.4 and 4.0, respectively, for heating provision in the coldest locality. The proposed multi-energy district reaches an electrical self-consumption of 71% in the coldest locality and efficiently combines different renewable energy sources at district level in cold climates.

Keywords

Multi-source energy systems, photovoltaic thermal panels, ground-source heat pump, low-temperature district heating network, renewable energy sources, energy district.

Nomenclature

a_1 [W/(m^2 K)]	Heat loss coefficient
a_2 [W/(m^2 K^2)]	Heat loss coefficient
b_{PV} [1/K]	Electrical loss coefficient
COP [kW/kW]	Coefficient of Performance
c_p [J/(kg K)]	Specific heat capacity
EE [kWh]	Electrical Energy
EER [kW/kW]	Energy Efficiency Ratio
G [kg/s]	Mass Flow Rate
I [W/m^2]	Solar Irradiance
L [m]	Length
η_0 [-]	Optical Efficiency
η_{el} [-]	Electrical Efficiency
$\eta_{ref\text{-}PV}$ [-]	Reference efficiency of PV
$\eta_{el,\ sys}$ [-]	Electrical efficiency of the system
Ω [m]	Pipe section perimeter
PEF [kWh]	Primary Energy Factor
PER [kWh]	Primary Energy Reduction
ρ [kg/m^3]	Density of the heat carrier fluid
SCOP [kWh/kWh]	Seasonal Coefficient of Performance
SEER [kWh/kWh]	Seasonal Energy Efficiency Ratio
T [°C]	Temperature
TE [MWh]	Thermal Energy
U [W/(m^2 K)]	Heat Transmittance Coefficient
V [m^3]	Volume
$W_{el,dem}$ [kWh]	Electrical energy demand
$W_{el,PVT}$ [kWh]	Self-generated solar power
$W_{el,PVT,tot}$ [kWh]	Electrical energy produced by the PVT field

Subscripts

a	Ambient
dem	Demanded
el	Electrical
HP	Heat pump
i	i-th node
j	j-th node
g	Undisturbed ground
max	Maximum
mean	Mean
min	Minimum
out	Exiting the component
PV	Photovoltaic
PVT	Photovoltaic Thermal
ref	Reference
sys	System
tot	Total

Abbreviations

4GDH	4th Generation District Heating
BHE	Borehole Heat Exchangers
COST	Costant
CTR	Control
CR	Coverage Ratio
DH	District Heating
DHW	Domestic Hot Water
DHC	District Heating and Cooling
DHN	District Heating Network
GSHP	Ground Source Heat Pump
HP	Heat Pump
LTDH	Low Temperature District Heating
MSES	Multi-Source Energy System
ODE	Ordinary Differential Equation
PV	Photovoltaic
PVT	Photovoltaic Thermal panel
SCOP	Seasonal Coefficient of Performance
SEER	Seasonal Energy Efficiency Ratio
SS	Supply Station
SUR	Self-Use Ratio
TRY	Test Reference Year
ULTDH	Ultra-Low-Temperature District Heating
VAR	Variable

1. Introduction

Lowering the energy use and decarbonizing the energy supply in the built environment are important environmental challenges of the upcoming decades. The electrification process, end-use energy efficiency and high share of renewable energy sources coupled to smart technologies offer opportunities to improve the energy efficiency in buildings and cities at small and large scale. In Section 1.1, the integration of multi-source energy systems in a single building is considered, starting from the small scale. In particular, the research works on combining photovoltaic thermal (PVT) with heat pumps for space are reported. In Section 1.2, the studies focused on the interconnection of renewable energy systems at the district level through low-temperature district heating (LTDH) networks are considered, moving to the large scale. Finally, in Section 1.3, the research work's novelty is presented.

1.1 Integration of multi-source energy systems in buildings

In this context, at the building level, multi-source energy systems (MSES) are rising interest as they can increase the exploitation of renewable energy sources, reduce the environmental impact related to the use of fossil fuels, and enhance the efficiency of heating and cooling systems. Emmi et al. [1] investigated a solar assisted ground source heat pump system in six cold locations. The results showed that when solar thermal collectors are not used, the seasonal energy performance of the heat pump decreased by about 10% over a ten year period. Instead, when solar energy was used, the seasonal energy performance was constant and above 4.5 over time. Significant research efforts focus on combining PVT panels with heat pumps for space heating and cooling application. A previous study [2] analyzed the energy performance of different MSES combinations coupled with PVT collectors and a heat pump. The investigated MSESs increased the energy efficiency by up to 25% over a conventional air-to-water heat pump system. Sommerfeld and Madani [3] studied a solar-assisted ground source heat pump system to describe its technical and economic potential for Swedish multi-family houses. The results showed that the PVT can reduce borehole length by 18% or spacing by 50% while maintaining an equivalent seasonal performance factor to systems without PVT. Bellos et al. [4] performed a techno-economic assessment of a PVT assisted heat pump for space heating in the building sector. The final result was that this system is more economically convenient than a PV coupled with an air source heat pump when the electricity price is higher than 0.23 €/kWh. A simulation model of a PVT assisted heat pump system for space heating or cooling and domestic hot water of a residential building was developed by Calise et al. [5]. An optimization aimed at minimizing the pay-back period of the energy system was performed, resulting in a simple pay-back period of 5.26 years. The latter decreased to 2.33 years, considering a capital investment incentive of 30%. However, a decrease in the system's performance was detected for weather conditions in which the availability of solar energy is scarce. Dannemand et al. [6] conducted an experimental analysis on a solar PVT assisted-heat pump system with a cold buffer storage tank and a domestic hot water storage tank; focusing on the interplay between the different components, the analysis indicated that the two-tank heat pump system was helped by the PVT collector.

1.2 Renewable energy systems at district level

The possibility of interconnecting these solutions fosters the development of sustainable energy districts. This is possible thanks to district heating and cooling (DHC) networks, essential urban infrastructures to enable the flexible integration of renewable energy and distributed generation systems. A prerequisite to their deployment is the reduction in the supply temperature of district heating networks (DHN) [7]. Lund et al. [8] developed the concept of low-temperature district heating, or 4th generation district heating (4GDH). The basic idea behind this concept is the reduction of both the distribution temperatures and pipe diameters to abate distribution heat losses and to allow the utilization of heat from distributed heating units such as prosumers. However, due to the relatively high temperatures, these systems are not well suited to allow a decentralized heat supply and the integration of lower temperature heat sources. In the last decade, around 40 DHC systems of the so-called 5th generation (5GDHC), or ultra-low-temperature district heating and cooling (ULTDHC) network were put in operation [9]. These networks operate at temperatures so close to the ground that they are not suitable for direct heating purposes. The low temperature of the carrier medium allows exploiting directly industrial and urban excess heat and the use of renewable heat sources at low thermal exergy content. The possibility to reverse the operation of the customer substations permits to cover simultaneously and with the same pipelines both the heating and cooling demands of different buildings.

ULTDHC technology enhances sector coupling of thermal, electrical and gas grids through hybrid substations in a decentralized smart energy system. In addition, Writz et al. demonstrated that ULTHC leads to substantially less total annualized costs (−42%), causes less carbon dioxide (CO2) emissions (−56%) and has a larger exergy efficiency compared to heating, ventilation and air conditioning (HVAC) systems [10]. Extra investment to the booster heat pumps enables savings in the distribution heat loss and utilization of low-grade energy sources. These heat pumps are installed in the customers' substations, and they raise the temperature of heat carrier fluid in the DHN according to the energy needs of the building served.

Examples of low temperature thermal grids coupled to borehole thermal energy storage with decentralized solar supply have been reported in a few projects such as the well-known Solar Drake Landing Community in Canada and the Suurstoffi district in Switzerland [11]. In Østergaard and Andersen [12], the performance of ULTDH is significantly better, compared to LTDH, in terms of both costs and primary energy demand for a theoretical case representing a typical small Danish DH network. An innovative low-temperature heating and cooling network, the district “Suurstoffi”, in Central Switzerland, was monitored by Vetterli et al. [13]. This case study is characterized by a large geothermal field, functioning as seasonal storage, with warm and cold ducts and PVT systems to operate the heat pumps. Chen et al. [14] evaluated the sustainability of a district heating system integrated with solar and geothermal sources, employing both vapour-compressor and absorption cycles through a ground source heat pump (GSHP) and an absorption heat pump (AHP) subsystem. A previous study conducted by Vivian et al. [15] investigated the advantages of ULTDH networks with booster heat pumps at the customers’ substations and their sensitivity to the main design parameters for a heating-only case study. Also Ommen et al. [16] conducted a theoretical investigation on the optimal use of booster HPs in ULTDH for new buildings. They found that the booster heat pumps can improve the system performance if a central heat pump (HP) is used for the heat supply of the network. Behzadi and Arabkoohsar [17] modelled and studied a novel solar-based building energy system on different district heating integration scenarios (existing, LTDH and ULTDH). In this case, the solar system, which uses PVT panels and has neither a battery nor a heat pump, is better suited for integrating with ULTDH than the existing network, or LTDH. In Garcia et al. [18], a hybrid system including PVT panels and a heat pump is proposed to provide domestic hot water (DHW), heating and electricity to a house located in central Europe. They demonstrated that the interaction of the proposed renewable-based system with the local DH system results in higher energy efficiency and reduced CO_2 emissions. Rosato et al. [19] investigated a centralized hybrid renewable district heating system based on the exploitation of solar energy and integrated with a seasonal borehole thermal energy storage. The energy system showed a reduction in primary energy consumption, equivalent carbon dioxide emissions, and operating costs of 11.3%, 11.7%, and 26.4% compared to a conventional decentarlized heating system, which is characterized by gas boilers. Pakere et al. [20] studied the optimal integration of PVT technology in district heating systems by covering industrial power consumption and heat demand of buildings in the Northern European climate.

1.3 Research novelty

The novelty of the present study consists of the new proposed energy system and the detailed analysis of its performance in different climates based on detailed physical models. In the dynamic simulations of the novel technical solution characterized by a ULTDH with booster HPs and PVT panels installed at the users level, the GSHP at the supply station is bypassed during the cooling season. The heat is directly released into the ground through the thermal storage that is connected to the borehole heat exchangers (BHEs). Moreover, previous research about integrating thermal prosumers in district heating networks is often carried out at a single building level, without considering the impact of decentralized heat supply on district-level indicators, such as the average return temperature, the electrical self-consumption, and the overall PVT performance. An example is the study of Emmi et al. [2], which demonstrated that a MSES equipped with PVT and a GSHP for the space heating and DHW production of a single-family dwelling located in North-East Italy determined an increase of energy efficiency of 16-25% compared to an air to water heat pump system. Furthermore, in another study, the MSES with PVT panels or solar thermal collectors in two different configurations were compared; as a result, a relevant improvement in the heat pump's efficiency using photovoltaic thermal panels was proved [21]. On the other hand, no analysis was performed at the district level in these studies, as carried out in this research work.

2. Methods

The study analyses a possible application of a ULTDH to an existing residential district. In a first step, this Section provides a qualitative description of the novel energy system and it is followed by a description of the simulation set up, including the simulation's steps, the boundary conditions and some consideration about the choice of the DHN supply temperature. Afterwards detailed explanations of the three main simulation's steps are reported, followed by the definition of some performance indicators of the considered energy plants, employed to evaluate the simulation results.

2.1 Description of the novel energy system

The energy system for the supply of heating, cooling, domestic hot water, and electrical energy is equipped with a rooftop PVT field and a reversible water to water heat pump installed in each residential district building. The solar field produces DHW and electricity for the apartments. Its electrical efficiency is enhanced as the DHN water is used to decrease the temperature of the PVT panels. Moreover, the DHN is employed as the source/sink for the heat pump. The DHN links the substations to the thermal storage in the Supply Station (SS), where GSHP releases heat during the heating season and that, through a direct connection to the BHE field, allows to reject the heat to the ground during the cooling season.

Figure 1 presents a simplified scheme of the energy system and its energy fluxes: for each building, yellow and red arrows represent the heat rejected to the DHN by the PVT panels and the heat pumps in cooling operation, while light blue dashed arrows show the heat that is extracted by the DHN in heating operation; between the DHN and the SS schemes, the dashed blue line is the return water temperature to the DHN and the blue line is the supply water temperature to the GSHP storage tank. In the same Figure 1, the grey arrows show the sequence of the simulation steps.

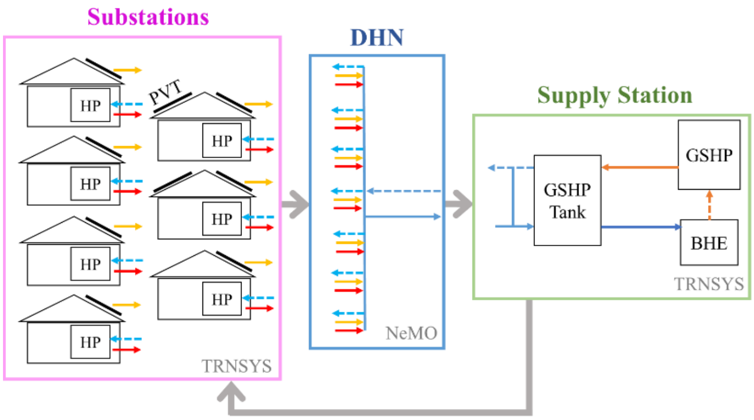

Figure 1. Scheme of the energy system and its energy fluxes.

2.2 Simulation set up

The analysis of the whole system, presented in Figure 1, involves an iterative simulation of the three main parts: the substations, the thermal network and the supply station. Concerning the modelling's steps, first, as the investigated residential district comprises 7 buildings, 6 units each, the detailed models of the 42 housing units, their plant systems, including the PVT fields and the heat pumps, are created. At this level, some boundary conditions are set: the climate conditions of the three investigated localities are used, and the temperature of the water circulating in the DHN, which has been determined with a parametric study, is assumed to be constant, differing only for the heating and cooling seasons. Afterwards, the temperatures of the water exiting the source side of the heat pumps and the PVT cooling tank in the substation are given as inputs to the DHN model, where the network's thermal inertia and thermal losses are considered. Consequently, the water mass flow rates and temperatures for each time step of the annual simulation are obtained, consisting of the inputs to the third part of the model, the SS. In this last section, the dynamic simulations of the GSHP, the thermal storage and the BHE are carried out, obtaining the values for the DHN inlet temperature. Finally, the temperature is kept at the desired value using a tempering valve at the outlet of the thermal storage tank, which is a thermostatic valve that maintains and limits the DHN water temperature by mixing the water from the GSHP storage tank with the return stream from the DHN.

The proposed technical solution was simulated for three cold locations, with the main aim of investigating the positive effects of the PVT panels integration to a ULTDHN in heating-dominant climates, which can lead to a mitigation of the thermal drift effect. The thermal drift effect is caused by unbalanced heat load to the ground in heating or cooling operations when using GSHP systems, and consists of a decrease/increase in the thermal potential of the soil for heat extraction/rejection, with consequent reduction of the energy performance of the installation. For the simulations, the Test Reference Year (TRY) data from the EnergyPlus database is used: the analysis is, therefore, carried out for Helsinki, Berlin and Strasbourg. For the substations and the DHN, the annual simulations are carried out with a time step of 15 minutes to evaluate the system's dynamic behaviour. The simulations of the SS are instead carried out considering 20 operating years, with a time step of 3 minutes, which allows avoiding convergence problems. The long simulation time is chosen to monitor the possible effect of the thermal drift on the temperature of the heat carrier fluid exiting the borehole heat exchanger field.

As for the supply temperature to the DHN, a parametric study was conducted to determine the most convenient temperature for the simulations. As mentioned, the water flowing in the DHN has a double function: it is used as the heat source/sink for the heat pumps of the substations and the cooling of the PVT panels. Therefore, different simulations were carried out at both the substations and SS levels, in order to identify the best couple of heating and cooling DHN set point water temperature. The main objective for the choice of the temperature levels was, indeed, to find a good compromise for enhancing the efficiencies of the heat pumps both in the supply station and in the substations, in heating mode and in cooling mode. In particular, the setpoint temperature was chosen as a consequence of the following aspects:

- the closer the temperatures of the heat source and the heat sink, the higher the efficiency of the reversible heat pumps in the substations: a higher supply temperature leads to higher efficiency during heating operation (space heating and DHW production) and a worse performance during the cooling season;
- a lower DHN water setpoint temperature improves the performance of the GSHP in the SS, which is switched on only during the heating season;
- during the cooling season, a lower network temperature leads to lower efficiency when producing DHW but increases the electricity production due to better cooling of the PVT panels.

A preliminary parametric analysis based on the considerations above has allowed setting the temperature of the network to 20°C and 25°C during the heating and cooling season, respectively.

In addition, a different strategy for enhancing the efficiency of the centralized GSHP was investigated, involving a variation of the DHN water temperature during the heating period: during the coldest months, from November to March, the supply temperature was kept at a constant value of 8°C, while during intermediate seasons, the temperature was set to 20°C. The obtained results are presented in Section 3.4.

2.3 Detailed building model including substations

The building envelope model is coupled to the plant model of the substations in the Simulation Studio workspace of TRNSYS 18 [22]. Concerning the buildings, they are well insulated and Table 1 summarizes the main thermal properties of the envelope of the buildings. The total volume of each building is equal to 2166 m^3, while the heated floor area is equal to 560 m^2.

Table 1. Thermal properties of the building envelope for the case study buildings.

	Thickness [cm]	**U-value [W/(m^2 K)]**
External Wall	42	0.19
Adjacent Wall	12	2.35
On Garage Floor	53	0.28
Intermediate Floor	54	0.44
External Roof	14	0.55
Windows	-	0.82

Internal gains related to the people occupancy and the use of domestic appliances, infiltrations and setpoint temperatures for heating and cooling are defined using the Standards ISO 18523-2:2018 [23] and ISO 7730:2005 [24]. The DHW load profiles throughout the year are evaluated employing DHWcalc [25], using default probability distributions and an average DHW consumption of 50 liters/person/day. Figure 2 reports a simplified scheme of the energy plants: dislocated in each building, a high-efficiency system is installed, consisting of a reversible water to water heat pump, a PVT field, a DHW tank for the DHW production, the space-heating and cooling radiant system and a PVT tank for the cooling of the PVT panels. Both the heat pump source side and the PVT tank exchange heat with the DHN. A novel TRNSYS Type, described in [26], is used to simulate the operating conditions of the heat pump based on polynomial curves describing the compressor's performance. The load-side of the booster heat pump is connected to the DHW tank to produce domestic hot water at a setpoint temperature of 43°C. The heat pump switches off when the temperature of the DHW tank reaches 45°C. This choice was made to limit the hot water temperature to the user to a reasonable value. Furthermore, the booster heat pump is connected to the radiant system of the building, which is provided considering a supply temperature of 33°C in heating and 18°C in cooling. The PVT field is installed on the south-facing roof slab for 5 of the 7 buildings, while its area is doubled and distributed on the east and west slabs of the roof for the remaining two buildings. The solar field is employed for the production of DHW and electricity. The model used for the PVT collectors refers to the research carried out by Zarrella et al. [27], and it is implemented by the same research group as a Type of TRNSYS software. The heat pump provides heat to the DHW tank when the thermal energy produced by the solar field is not sufficient to reach the setpoint. When there is no need for thermal energy production from the PVT field, as the temperature of the water inside the DHW tank is already at the setpoint, and the temperature of the PV surface is above 35°C (with a dead band of 1.5°C), the PVT field is cooled down, exchanging heat with the PVT tank, through a heat exchanger, which is linked to the DHN.

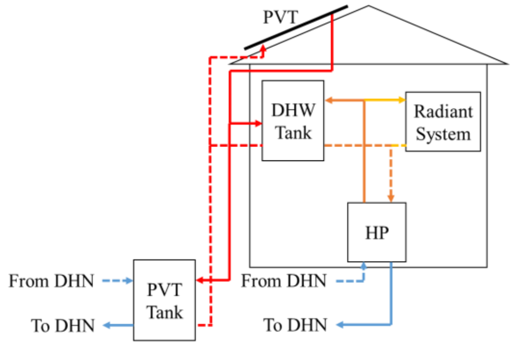

Figure 2. Sketch of the energy plant at the substations.

For the heat pump, a size of 36 kW is chosen for the buildings in Helsinki, of 25 kW in Berlin and Strasbourg, based on the thermal loads computed for the analyzed case studies. The tanks have the same volume for the different case studies, equal to 800 liters for the DHW tank and 450 liters for the PVT tank. The PVT field has an overall PV area of 57.6 m^2 and a module area of 66.4 m^2 for the north-oriented buildings, while it is doubled for the buildings whose slabs are east- and west-oriented with a slope of 45°. The thermal efficiency of the PVT panels is expressed in Equation (4) [28].

$$\eta_{th} = \eta_0 - a_1(T_{mean} - T_a)/I - a_2(T_{mean} - T_a)^2/I \quad (4)$$

where η_0 is the zero-loss efficiency (set to 0.7), a_1 and a_2 heat loss coefficients (set to 12 W/(m^2 K) and 0 W/(m^2 K^2), respectively), T_{mean} is the mean temperature of the heat transfer fluid, T_a is the ambient temperature, and I (W/m^2) the solar irradiance. The values of the coefficients used in the model are derived from datasheets of commercial panels. The PVT electrical efficiency is a function of the mean temperature of the PV layer, and the electrical power production is calculated using Equation (5) [24]. The value of the coefficient η_{ref-PV}, which can usually be found in the datasheet of the PV or PVT module, represents the efficiency of the PV module at the reference temperature T_{ref-PV} = 25°C (standard test conditions). The coefficient b_{PV} is then used to consider the deviation from the reference values and A is the area of the PV panels: this coefficient is set to 0.0045 K^{-1}.

$$P_{el} = I \cdot A \cdot \eta_{ref-PV} \cdot [1 - b_{PV}(T_{PV} - T_{ref-PV})] \quad (5)$$

2.4 District heating network model

A scheme of the ULTDH system under consideration, operating at constant supply temperature and variable flow rate, is shown in Figure 3. The network is about 450 m long. The blue dots are the connection nodes between the pipes of the DHN, while the orange dot represents the supply station in which the centralized GSHP is installed. Each of the seven buildings is provided with one heat pump and a PVT field on the roof: the red and light blue dots indicate the HPs when they respectively supply or withdraw heat from the network, while the yellow dots represent the PVT systems, which provide heat to the network when the photovoltaic panels are cooled.

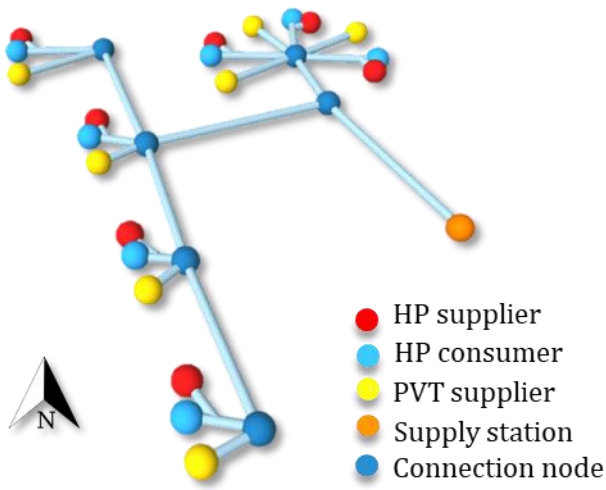

Figure 3. Scheme of the considered district heating and cooling network.

The network is mathematically represented by a set of nodes and oriented branches, and an adjacency matrix determines their mutual connections. Figure 4 shows the generic *i-th* node connected to an upstream (j-1) and downstream (j) branch.

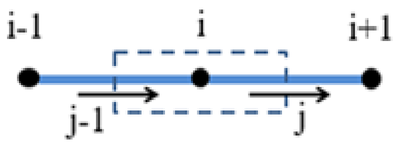

Figure 4. Control volume of the i-th node.

Once the geometry is established, the pressure and temperature profiles are calculated. In problems of forced convection, the velocity of the heat carrier fluid does not depend on the temperature distribution. Therefore, the hydraulic and thermal problems can be uncoupled. This allows performing the calculation of the mass flow rates and the pressures across the network; subsequently, given the mass flow rates, the energy balance is solved to determine the temperature distribution. The model assumes a plug flow (one-dimensional model) and neglects both the heat conduction in the axial direction and the heat capacity of the surrounding ground. The heat transfer in the radial direction considers the convection between the heat carrier fluid and the inner pipe surface, the pipe's thermal insulation, and the thermal resistance of the surrounding ground.

Due to the incompressible nature of the heat carrier fluid, the hydraulic problem can be described using only two equations: the continuity and the momentum equations. NeMo solves these equations using the SIMPLE method [29].

The heat propagation in the network is then described by the energy balance performed on the volume of heat carrier fluid around the nodes of the network. The control volume of the *i-th* node corresponds to half of the heat carrier fluid volume of all the branches connected to it. Applying the energy balance to the node shown in Figure 4 leads to Equation (6):

$$\rho V_i c_p \frac{\partial T_i}{\partial t} = G_{j-1} c_p T_{j-1} - G_j c_p T_j - \frac{1}{2}\left(L_j \Omega_j U_j + L_{j-1} \Omega_{j-1} U_{j-1}\right)(T_i - T_g) \quad (6)$$

where *G* is the mass flow rates, *V* is the volume of heat carrier fluid enclosed in the control volume, **Ω** is the perimeter of the pipe section, *U* is the radial heat transmission coefficient from fluid to the ground, and T_g is the undisturbed ground temperature. The temperature of the branches is then associated with the temperature of the corresponding upwind nodes, according to the upwind scheme. Therefore, Equation (6) becomes:

$$\rho V_i c_p \frac{T_i^{(t)} - T_i^{(t-\Delta t)}}{\Delta \tau} = G_{j-1} c_p T_{i-1}^{(t)} - G_j c_p T_i^{(t)} - \frac{1}{2}\left(L_j \Omega_j U_j + L_{j-1} \Omega_{j-1} U_{j-1}\right)\left(T_i^{(t)} - T_g\right) \quad (7)$$

Equation (7) can be represented in matrix form as:

$$M\,\dot{T} = s - K\,T \quad (8)$$

where *M* and *K* are the so-called mass matrix and stiffness matrix, respectively. The temperature at the inlet node is fixed (Dirichlet condition) and the missing mass is attributed to the adjacent nodes. The first-order ordinary differential equation (ODE) (8) can be rewritten to give a linear system that can be solved by Gauss elimination method, as shown in Equation (9) and (10):

$$\frac{M}{\Delta t}\left(T - T_{-\Delta t}\right) = s - K\,T \quad (9)$$

$$\left(K + \frac{M}{\Delta t}\right) T = \left(s + \frac{M}{\Delta t} T_{-\Delta t}\right) \quad (10)$$

where $T_{-\Delta t}$ represents the temperature vector with the temperature values of the preceding time-step (initial network temperature at the beginning of the simulation). In the current version of the model NeMo, the user can choose the resolution method for the transient heat propagation problem between the ODE solver (Equation 8) and the linear system solver (Equation 10). The latter allows the user to set the time-step of the internal solver Δt. A full description of the model is given in [30].

2.5 Thermal model of the supply station

The model of the SS is simulated in the TRNSYS environment. A scheme of the simulated system can be seen in Figure 5, where the configurations used during the heating (a) and cooling (b) seasons are summarized. In order to guarantee the setpoint temperature at the source-side of the heat pumps and the PVT tanks in the substations, a centralized GSHP releases heat to a GSHP tank through an immersed heat exchanger. A tempering valve is used to mix the return DHN stream with the water mass flow rate exiting the GSHP tank port to obtain the desired outlet temperature.

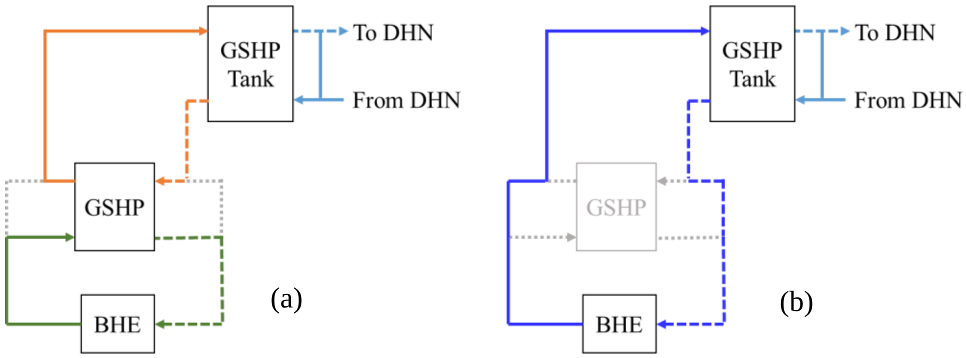

Figure 5. Scheme of the centralized GSHP system during the heating (a) and cooling (b) seasons.

The GSHP is modeled using the novel TRNSYS Type mentioned in the previous paragraph, using the compressors' polynomials of machines with a rated heating capacity of 135 kW for the case study of Helsinki, 96 kW for Berlin and Strasbourg. An initial assessment of the borehole heat exchanger (BHE) field size was done using the ASHRAE [31] method. It resulted in BHEs' number (100 m long each) equal to 98 for Helsinki, 36 for Berlin and 32 for Strasbourg. However, for the analyzed plant configuration, the number of boreholes can be reduced to the values reported in Table 2. The BHEs are simulated using TRNSYS Type 557a. The main properties of the borehole field are presented in Table 2. For the ground thermal conductivity, the same value equal to 2.2 W/(m K) was assumed for the three different locations as a simplification. The aim is to consider the same ground boundary conditions and compare the results in the three locations.

Table 2. Main characteristics of the BHE field.

	Helsinki	**Berlin**	**Strasbourg**
Ground			
Specific heat	1000 J/(kg K)		
Density	2500 kg/m^3		

Undisturbed temperature	5.2 °C	9.8 °C	10.2 °C
Thermal conductivity	2.2 W/(m K)		
Thermal gradient	0.03 °C/m		
Specific volume heat capacity	2500 kJ/(m^3 K)		
Pipe			
Length of each borehole	100 m		
Number of Boreholes	75	35	30
Thermal conductivity	0.35 W/(m K)		
Outer/Inner diameter of pipe	32/26 mm		
Center-to-center distance	78 mm		
Distance between BHEs	8 m		
Fluid			
Composition	Water-Glycol (30%)		
Specific heat	3.915 kJ/(kg K)		
Density	1031 kg/m^3		

During the cooling season, as the ground temperature is low enough to cool the GSHP Tank at the chosen supply temperature, the heat pump is bypassed, and the immersed heat exchanger of the GSHP Tank is directly connected to the BHE field (Figure 5b). This configuration can be employed because the analyzed case studies are characterized by cold climate conditions and, therefore, by low cooling thermal loads of the buildings and low mean temperatures of the ground: the BHE can be directly used to cool the water inside the storage tank at the set temperature level.

2.6 Evaluation of energy system performance

Five performance indicators have been considered to evaluate the energy performance of the novel solution for providing space heating, cooling and domestic hot water to the district. One is the Coverage Ratio (CR), which represents the percentage of electrical energy demand ($W_{el,dem}$) covered by the self-generated solar power ($W_{el,PVT}$) using the PVT panels.

$$CR = \frac{W_{el,PVT}}{W_{el,dem}} * 100 \qquad (1)$$

Similarly, the Self-Use Ratio (SUR) indicates the percentage of the overall electrical energy produced by the PVT field ($W_{el,PVT,tot}$) that is self-consumed by the considered system. The latter includes the heat pumps, the electrical appliances in the network's substations and the GSHP of the supply station, considering the concept of the energy community. Otherwise, the electrical production of the PVT panel installed on the roof of each building is considered for meeting the demand of the same substation (appliances and heat pump). The electrical energy produced by the PVT field, is released to the electrical grid, is not considered by the SUR.

$$SUR = \frac{W_{el,PVT}}{W_{el,PVT,tot}} * 100 \quad (2)$$

Another indicator related to PVT performance is the Primary Energy Reduction (PER), which represents the reduction of primary energy consumption determined by the self-consumption of the electrical energy produced by the PVT systems.

$$PER = W_{el,PVT} * PEF \quad (3)$$

Where PEF is the Primary Energy Factor according to Sartori et al. [32]. For Finland (Helsinki) and Germany (Berlin), the PEF values are respectively 1.7 and 3, while for France is 2.58 [33].

The heat pumps' energy performances are evaluated in terms of seasonal coefficient of performance (SCOP) and seasonal energy efficiency ratio (SEER). The SCOP is the annual thermal energy exchanged at the heat pump's condenser during heating operation ($Q_{heating,HP}$), divided by the electrical energy absorbed by the compressor ($W_{el,HP}$).

$$SCOP = \frac{Q_{heating,HP}}{W_{el,HP}}$$

Correspondingly, for cooling operation, the SEER is the annual thermal energy that is extracted in the evaporator at the load side of the heat pump ($Q_{cooling,HP}$), divided by the electrical energy absorbed by the compressor ($W_{el,HP}$).

$$SEER = \frac{Q_{cooling,HP}}{W_{el,HP}}$$

3. Results and discussion

This section presents the results obtained from the simulations at the substations and the supply station levels. Moreover, considerations about the electrical and primary energy at a district level are provided. Finally, the results regarding the use of two temperature levels for the DHN water during the heating season are reported.

3.1 Substations: the simulation results

The monthly thermal energy demanded by the buildings for space heating, space cooling, and DHW production is illustrated in Figure 6. The thermal loads for all the considered climates are heating-dominant, with a heating/cooling ratio equal to 4.1 for Helsinki, 2.3 for Berlin and 1.5 for Strasbourg. Correspondingly, in Table 3, the annual and specific (related to the heated floor area) values for the thermal energy demand of heating, cooling and DHW are shown.

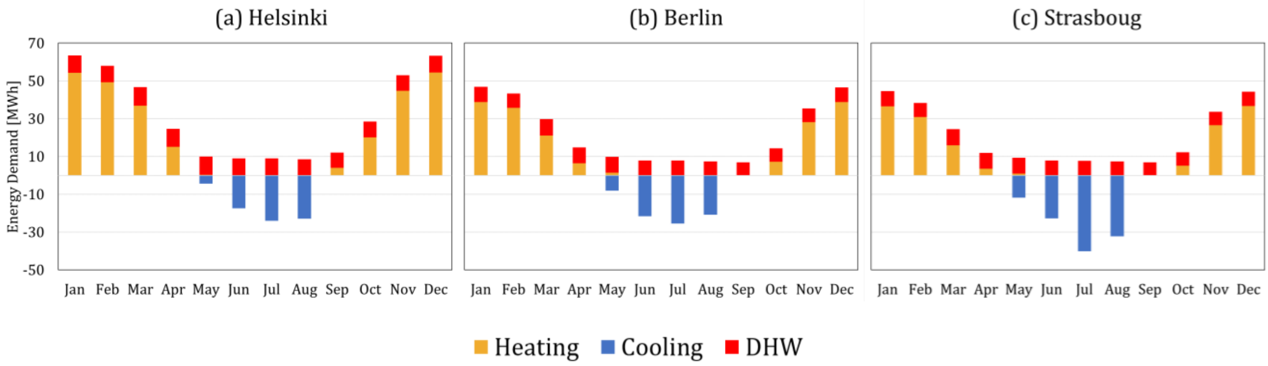

Figure 6. Monthly thermal energy demanded by the neighbourhood for heating (orange), cooling (blue) and DHW production (red) for (a) Helsinki, (b) Berlin and (c) Strasbourg.

Table 3. Annual and specific thermal energy demanded by the neighbourhood for heating, cooling and DHW production for the three localities.

	Heating		**Cooling**		**DHW**	
	[MWh]	[kWh/m^2]	[MWh]	[kWh/m^2]	[MWh]	[kWh/m^2]
Helsinki	279.38	71.3	-68.81	-17.6	106.53	27.2
Berlin	177.57	45.3	-75.96	-19.4	93.57	23.9
Strasbourg	156.34	39.9	-106.94	-27.3	92.44	23.6

The DHW demand is computed considering a setpoint temperature of 43°C and a temperature of the municipality water that differs between the three localities and depends on the mean annual temperature of the external air. In particular, concerning the DHW production, which has priority over space heating and cooling provision, Table 4 reports the share of thermal energy for the production of DHW, released by the solar field and by the heat pumps for the three investigated localities. As expected, it can be noticed that in Helsinki (the coldest locality), the total energy need is higher than for the other case studies, while the PVT thermal production is lower (up to 34% lower than in Strasbourg). This means that the contribution of heat pumps is more relevant in Helsinki and, in particular, 28% higher than in Strasbourg.

Table 4. Total thermal energy for the DHW production by PVT field and HPs contribution

	PVT		**HP**		**Total**
Helsinki	17.7 MWh	16%	92.9 MWh	84%	110.6 MWh
Berlin	20.0 MWh	21%	77.0 MWh	79%	97.1 MWh
Strasbourg	23.8 MWh	25%	72.0 MWh	75%	95.8 MWh

Table 5 presents the electrical energy absorbed by the heat pumps and their performance when operating in cooling mode and in heating mode for space heating and DHW production. The performance is evaluated in terms of SCOP and SEER. Overall, on an annual basis, the electrical energy absorbed by the heat pumps in the substations for the three case studies is around 91 MWh in Helsinki, 71 MWh in Berlin and 73 MWh in Strasbourg. It can be observed that this value is higher for the case of Helsinki, where the thermal load for heating and DHW provision is 46% and 62% higher than for Berlin and Strasbourg, respectively. On the other hand, Berlin presents an electrical consumption that is slightly lower than in Strasbourg due to a cooling load that is 41% higher for this last case study.

Table 5. Electrical energy demanded by the heat pump and performances in the substations.

	Electrical Energy Demanded [kWh]			**SCOP/SEER** [kWh/kWh]		
	Heating	**Cooling**	**DHW**	**Heating**	**Cooling**	**DHW**
Helsinki	50303	13947	26967	5.4	4.9	3.7
Berlin	33004	16798	21795	5.2	4.5	3.8
Strasbourg	29096	23529	20404	5.2	4.6	3.8

The heat pumps are very efficient, and their performance values are similar for the different localities, as the temperatures of the heat sources and sinks are constant. In particular, as the same compressor model is chosen for the cases of Berlin and Strasbourg, the values for the SCOPs and SEERs do not change for these two localities, unlike for the case of Helsinki, where different performances characterize the machine. Considering the production of the solar field, Table 6 reports the thermal energy produced by the PVT panels installed in the district and released to the DHW tank or to the DHN. Moreover, it shows the electrical energy production and the overall electrical efficiency of the PVT field.

Table 6. Thermal energy (TE) produced by the solar field and released to the DHW tank and to the DHN, electrical energy (EE) production and electrical efficiency (η_{el}) of the PVT field.

	TE to DHW Tank [MWh]	**TE To DHN** [MWh]	**EE** [MWh]	$\boldsymbol{\eta_{el}}$
Helsinki	16.81	17.02	112.18	17.9%
Berlin	20.14	18.42	111.35	17.6%
Strasbourg	23.90	21.23	118.98	17.4%

The cooling of the PVT panels allows obtaining slightly higher electrical efficiencies, as the electrical production increases with the reduction in the temperature of the PV cells. Figure 7 shows this effect during a representative summer day for a building in Berlin. In Figure 7, the temperature of the cells, which is an output of the PVT capacitive TRNSYS type, is reported for the case with (blue line) and without (yellow line) PVT cooling. When the PVT cooling control is active, that is when the graph area is filled in green colour, the curves for the PV cells' temperatures diverge; correspondingly, the effect of the electrical efficiency rise can be noticed. The electrical efficiency is shown with red dots for the case without PVT cooling and with blue dots for the case with PVT cooling. When the PVT cooling control is active, on average the electrical efficiency of the PV cells rises from a value of 16.2% to 16.5%, leading to an increase in the electrical energy production of 512 kWh in one year.

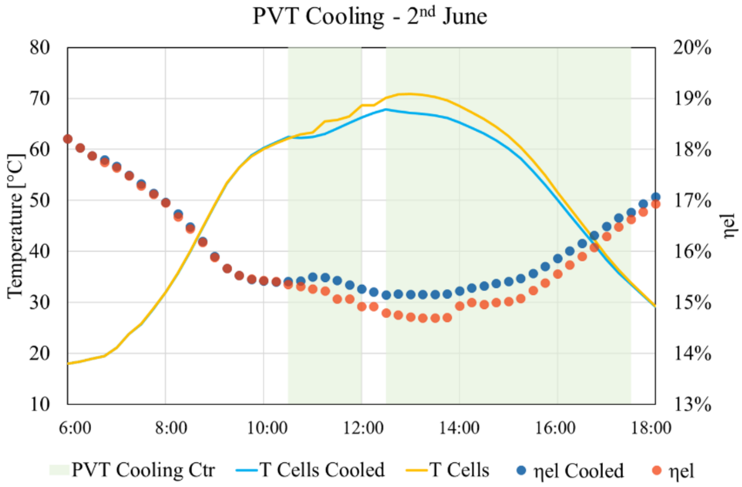

Figure 7. Berlin - PVT cooling control (green area), PV cells' temperatures and electrical efficiency for the cases with ("cooled" in the graph) and without PVT cooling.

Table 7 presents the annual thermal energy withdrawn from (+) or released to (-) the DHN. In particular, the energy is divided between the contribution related to the HPs operation and the PVT cooling. The PVT field contributes to reducing the thermal energy extracted from the DHN during the cold season, while during the warm season, as the district loads are heating-dominant, it increases the heat fluxes released to the DHN and, consequently, favours the balancing of the thermal load at the ground. For example, when considering the difference between the net thermal energy overall extracted from the DHN during the cold season and the energy released during the warm season, this value amounts to 158.7 MWh in Helsinki, 63.5 MWh in Berlin and 10.4 MWh in Strasbourg. On the other hand, if the PVT contribution is not considered, the net thermal energy to the DHN becomes equal to 176.4 MWh in Helsinki, 83.9 MWh in Berlin and 66.5 MWh in Strasbourg, demonstrating an influence of the PVT field on the thermal load unbalance.

Table 7. Thermal energy released to (-) and extracted from (+) the DHN during the cold and the warm seasons.

	Cold Season [MWh]			**Warm Season** [MWh]		
	HP	**PVT**	**HP-PVT**	**HP**	**PVT**	**HP+PVT**
Helsinki	276.8	-3.6	273.2	-101.1	-13.5	-114.6
Berlin	186.6	-5.0	179.2	-102.7	-13.0	-115.7
Strasbourg	167.4	-5.4	159.3	-133.8	-15.2	-149.0

For concluding the evaluation of the substations energy systems, Figure 8 shows the intraday effects on the SS return temperature due to the HP sink/source fluctuations and the PVT behaviour in each substation for a representative summer day in Berlin. In Figure 8, negative values for the thermal power mean that the network supplies heat to the HPs in the substations to produce DHW. On the contrary, positive values stand for space cooling demand or PVT cooling, leading to heat rejection to the network. The PVT contributions concentrate between 10 am and 8 pm and determine a high increase in SS return temperature, reaching 31°C at 3 pm, whereas the supply temperature is constant at 25°C. On the other hand, the operations of heat pumps are managed differently in the different buildings, resulting in minor variations of SS return temperature.

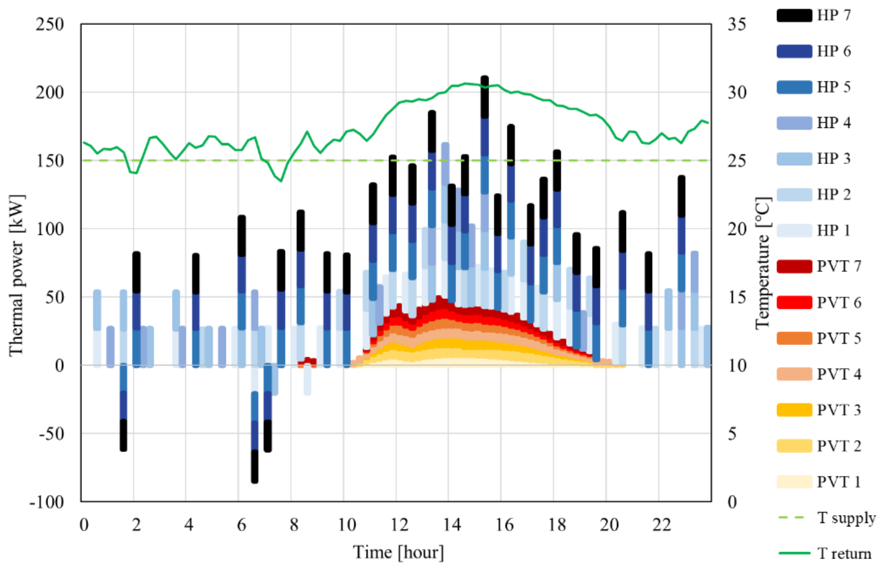

Figure 8. Intraday effects on the SS return temperature due to the HP and PVT cooling for a summer day (2nd June).

3.2 Supply station: the simulation results

The simulations carried out at the supply station level give information about the behaviour of the GSHP, which is connected to the DHN through the GSHP Tank and to the borehole field. The main output of this step of the modelling is the heat exchanged between the SS and the DHN. Figure 9 shows the monthly energy exchanged between the GSHP tank and the DHN, where positive values represent the energy released to the DHN, while negative values the heat that is extracted from the DHN.

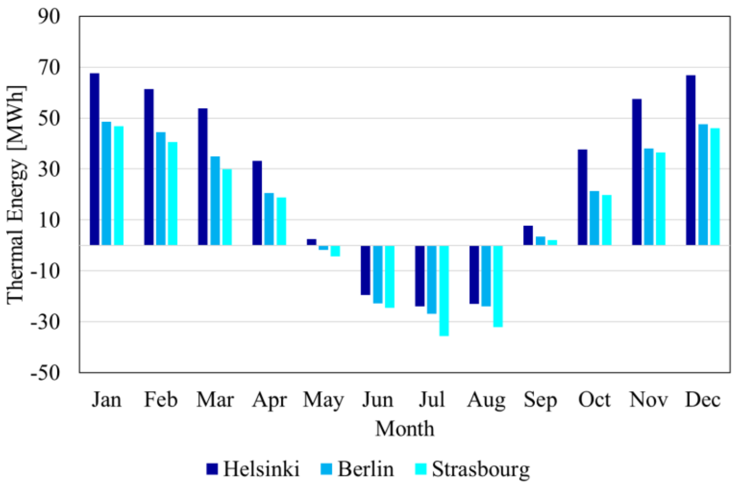

Figure 9. Monthly values for thermal energy exchanged between the GSHP Tank and the DHN.

As anticipated, the simulation time was set to 20 years and allowed to monitor the operation of the GSHP. Indeed, the machine's performance might change over time due to the thermal drift effect of the ground, related to the unbalanced thermal load conditions. Figure 10 shows the trend along 20 years of the monthly COP for the three localities, decreasing with a tendency that depends on the BHE outlet temperature drop. Therefore, in Figure 10, the annual minimum and maximum temperatures of the heat carrier fluid exiting the BHE field are given as a reference. The SCOP varies from 4.0 for the first year of operation to 3.7 for the 20th year in Helsinki, from 5 to 4.7 in Berlin and from 4.8 to 4.5 in Strasbourg.

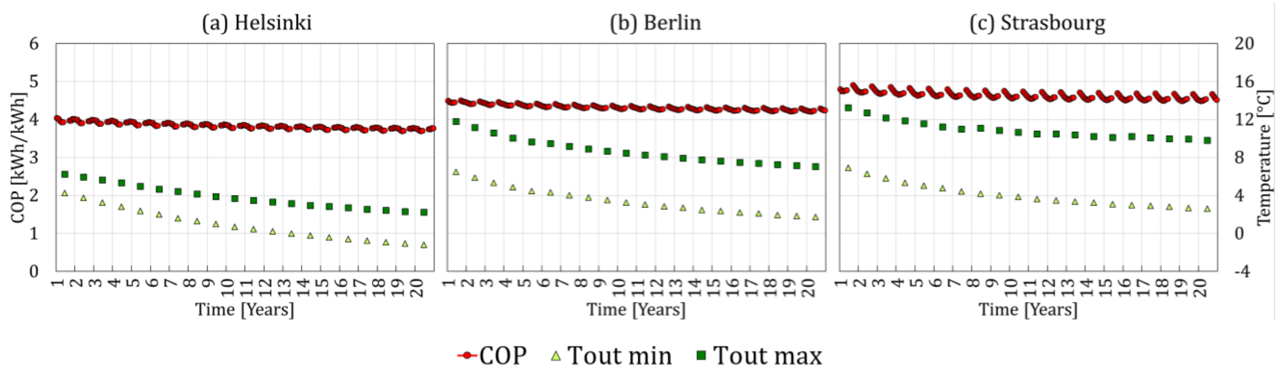

Figure 10. Monthly COPs, annual minimum (Tout min) and maximum (Tout max) outlet fluid temperatures at the BHE field for (a) Helsinki, (b) Berlin and (c) Strasbourg.

During the first year, the electrical demand of the GSHP is equal to 100.1 MWh in Helsinki, 54.5 MWh in Berlin and 53.4 MWh in Strasbourg. For the case without PVT cooling, in Berlin, the electrical energy consumption of the centralized GSHP, providing the same thermal load to the GSHP Tank, would rise to 54.8 MW. Between the 1st and the 20th year of operation, the electrical demand of the GSHP on annual basis increases by 3.1 MWh for the case with PTV cooling and 3.4 MWh for the case without PVT cooling in Berlin. Moreover, evaluating the PVT electrical output, during one year an additional difference of 460 kWh in the production can be obtained if PVT cooling is considered.

3.3 Electrical and primary energy considerations at the district level

The electrical production of the PVT field contributes to meeting the demand of the plant related to the electrical consumption of the heat pumps in the substations, the consumption of the electrical appliances in the buildings and the GSHP demand. If the electrical production of the solar field installed on the roof of each building was considered for meeting the demand of the same substation (appliances and heat pumps), the CR would be 29% in Helsinki, 30% in Berlin and 32% in Strasbourg. In the same context, the SUR would be around 64% in Berlin and Strasbourg, 66% in Helsinki. On the other hand, introducing the concept of energy community, where although the solar field is distributed on the different roofs, it belongs to the whole district, its production can increase the SUR of the system. Indeed, also considering the GSHP electrical demand, with this perspective the SUR increases to 71% for Helsinki and Berlin case studies and 70% for Strasbourg. Concerning the energy community concept, Figure 11 shows the electrical energy consumption by use, the production of the whole solar field in the district, the CR and the SUR. In this configuration, the CR would be 22% in Helsinki, 27% in Berlin and 28% in Strasbourg. The annual electrical energy that the grid must provide amounts to 261 MWh for Helsinki, 196 MWh for Berlin and 192 MWh for Strasbourg. On the contrary, the energy produced by the solar field but exceeding the plant's electrical demand is about 29 MWh for Helsinki and Berlin, 32 MWh for Strasbourg. Finally, in one year, the electrical energy produced by the PVT systems at the district level involves a PER of 212 MWh for Berlin, and it is equal to 122 MWh and 113 MWh, respectively for Helsinki and Strasbourg. The values for the solar field electrical production reported in Figure 11 and the related calculations of CR and SUR consider an electrical efficiency of 0.9 due to the electrical plant components' losses (i.e. the inverter).

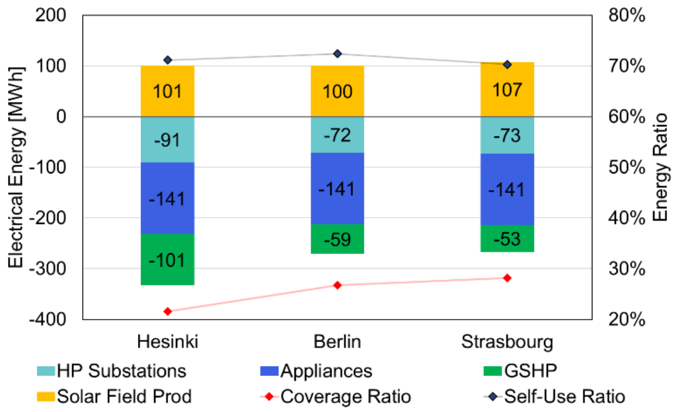

Figure 11. Electrical energy consumption by use and coverage and self-use ratio at district level.

3.4 Effect of the variation in the district heating network water temperature during the heating period

As anticipated in Section 2.2, a different strategy for enhancing the efficiency of the centralized GSHP was investigated for Berlin climate, since this location is characterized by intermediate weather conditions, compared to Helsinki and Strasbourg. During the heating period, the supply temperature was kept at a constant value of 8°C from November to March, while during intermediate seasons, the temperature was set to 20°C. For these simulations, the water temperature in the DHN is always at 25°C during summer. The temperature of 8°C was chosen as it is closer to the average temperature of the ground in Berlin and leads to lower energy consumption of the centralized GSHP.

As expected, during the coldest months, the decrease in the supply temperature leads to a decrease in the performance of the substations' heat pumps. Figure 12 shows the monthly COP for heating and DHW production, together with the supply temperature level. As expected, the performance is higher during the middle seasons' months, when the DHN water temperature is at 20°C.

Overall, the electrical energy consumption related to the operation of the substations' heat pumps for the provision of heating and DHW increases by 8.5% compared to the case with a constant temperature of 20°C during the whole heating period, with a value of 59.5 MWh.

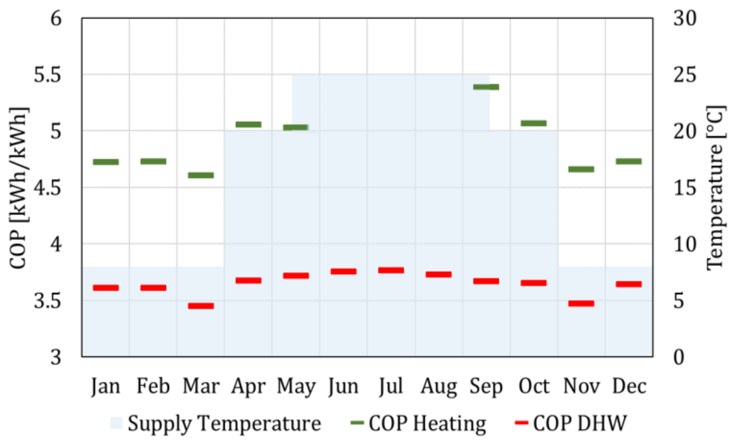

Figure 12. Berlin - Substation heat pumps monthly COP for the provision of space heating and DHW and supply setpoint temperature from the DHN.

On the other hand, during the first year of operation, it is possible to obtain a relevant decrease in the electrical energy demanded by the centralized GSHP, equal to 45.1 MWh during the first year, reaching a saving of 21%. This is because the lower supply temperature allows a decrease in the temperature of the water contained inside the thermal storage in the SS, reducing the thermal load to be delivered by the GSHP.

Figure 13 shows a comparison between the case with constant DHN water temperature setpoint and variable setpoint. In particular, Figure 13 shows the supply water temperature after being mixed with the return water temperature from the network, and the monthly values of the GSHP COP, for both the cases with constant heating setpoint temperature and variable heating setpoint temperature. The monthly COP, when the setpoint temperature is equal to 8°C is significantly higher than the case with supply temperature at 20°C.

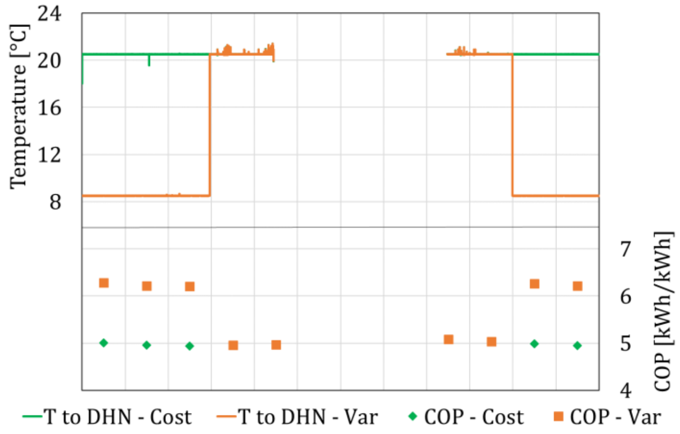

Figure 13. Berlin - GSHP monthly COP and supply water temperature to DHN.

In conclusion, concerning the CR and the SUR, the results are similar than for the case with constant setpoint. Indeed, if the electrical production of the solar field is used to meet the demand in the same substation (appliances and heat pumps), the CR would be 30% and the SUR 64%. On the contrary, if the PV production was used for the whole energy community the CR would be 27% and the SUR 71%. The annual electrical energy that the grid must provide amounts, in this case, to 191 MWh, while the energy produced by the solar field but exceeding the plant's electrical demand is about 30 MWh.

4. Conclusions

A technical solution for supplying heating, cooling, domestic hot water and electrical energy to a small residential district is investigated in three locations: Helsinki, Berlin and Strasbourg. The buildings are equipped with rooftop PVT systems and a reversible water-to-water heat pump that can extract/supply heat from/to an ultra-low temperature district heating network. During the heating season, the network is supplied by a high-efficiency GSHP.

The simulations performed at building level show that in the coldest climate (Helsinki), the PVT covers 16% of the total thermal energy needed for the DHW production. The booster heat pump supplies the remaining part. In Strasbourg, which is characterized by a warmer climate, the PVT contribution for DHW production reaches 25%. The heat pumps show high efficiency in cooling mode (SEER = 4.9) and heating mode for space heating (SCOP = 5.4) and DHW (SCOP = 3.7). As the temperatures of the heat sources and sinks are constant, these values are similar for the different localities.

The simulations of the GSHP coupled to borehole heat exchangers, give information about the long-term performance of the system, considering the thermal drift effect of the ground over 20 years. In Helsinki, the SCOP does not change significantly, i.e. from 4.0 for the first year of operation to 3.7 for the 20th year. This variation is reduced thanks to the PVT panels that help balance the thermal load at the ground, reducing the thermal energy extracted from the DHN during the cold season and increasing the heat fluxes released to the DHN during the warm season. At the same time, the electrical production of the PVT field increases thanks to the cooling of the PV cells. Finally, the self-consumed electricity is equal to 71% for Helsinki and Berlin and 70% for Strasbourg compared to the overall electricity production from the PVT systems.

A different strategy for enhancing the efficiency of the centralized GSHP was also investigated for the intermediate climate, Berlin. During the heating period, the supply temperature was decreased compared to the reference case, during the coldest months. Despite leading to an overall increase of 8.5% in the electrical demand at the substations' level, this solution allows obtaining a reduction in the centralized GSHP electrical consumption of 21%.

In conclusion, the study presents an overview on the performance of a low-temperature district grid integrated with renewable energy technologies such as PVT systems and borehole heat exchangers. The proposed solution appears attractive for small residential areas in cold climates. In addition, the research highlights how detailed models can be integrated with each other, leading to accurate district-level analysis. Future works could also include the effect of auxiliary devices on performance and electrical demand of the system, such as circulators in the ground loop and DHN. Moreover, it would be interesting to perform some dynamic control on the setpoint temperature of the network, that might change along the year and the lifetime of the energy plant, to adapt to performance degradation of the system for long term operation.

References

[1] Emmi G, Zarrella A, De Carli M, Galgaro A. An analysis of solar assisted ground source heat pumps in cold climates. Energy Convers Manag 2015;106:660–75. https://doi.org/10.1016/j.enconman.2015.10.016.

[2] Emmi G, Zarrella A, De Carli M. A heat pump coupled with photovoltaic thermal hybrid solar collectors: A case study of a multi-source energy system. Energy Convers Manag 2017;151:386–99. https://doi.org/10.1016/j.enconman.2017.08.077.

[3] Sommerfeldt N, Madani H. In-depth techno-economic analysis of PV/Thermal plus ground source heat pump systems for multi-family houses in a heating dominated climate. Sol Energy 2019;190:44–62. https://doi.org/10.1016/j.solener.2019.07.080.

[4] Bellos E, Tzivanidis C, Moschos K, Antonopoulos KA. Energetic and financial evaluation of solar assisted heat pump space heating systems. Energy Convers Manag 2016;120:306–19. https://doi.org/10.1016/j.enconman.2016.05.004.

[5] Calise F, Dentice d'Accadia M, Figaj RD, Vanoli L. Thermoeconomic optimization of a solar-assisted heat pump based on transient simulations and computer Design of Experiments. Energy Convers Manag 2016;125:166–84. https://doi.org/10.1016/j.enconman.2016.03.063.

[6] Dannemand M, Perers B, Furbo S. Performance of a demonstration solar PVT assisted heat pump system with cold buffer storage and domestic hot water storage tanks. Energy Build 2019;188–189:46–57. https://doi.org/10.1016/j.enbuild.2018.12.042.

[7] Connolly D, Lund H, Mathiesen B V, Werner S, Möller B, Persson U, et al. Heat Roadmap Europe: Combining district heating with heat savings to decarbonize the EU energy system 2013. https://doi.org/10.1016/j.enpol.2013.10.035.

[8] Lund H, Werner S, Wiltshire R, Svendsen S, Thorsen JE, Hvelplund F, et al. 4th Generation District Heating (4GDH): Integrating smart thermal grids into future sustainable energy systems. Energy 2014;68:1–11. https://doi.org/10.1016/J.ENERGY.2014.02.089.

[9] Buffa S, Cozzini M, D'Antoni M, Baratieri M, Fedrizzi R. 5th generation district heating and cooling systems: A review of existing cases in Europe. Renew Sustain Energy Rev 2019;104:504–22. https://doi.org/10.1016/j.rser.2018.12.059.

[10] Wirtz M, Kivilip L, Remmen P, Müller D. 5th Generation District Heating: A novel design approach based on mathematical optimization. Appl Energy 2020;260. https://doi.org/10.1016/j.apenergy.2019.114158.

[11] Sibbitt B, McClenahan D, Djebbar R, Thornton J, Wong B, Carriere J, et al. The Performance of a High Solar Fraction Seasonal Storage District Heating System – Five Years of Operation. Energy Procedia 2012;30:856–65. https://doi.org/10.1016/J.EGYPRO.2012.11.097.

[12] Østergaard PA, Andersen AN. Booster heat pumps and central heat pumps in district heating. Appl Energy 2016;184:1374–88. https://doi.org/10.1016/j.apenergy.2016.02.144.

[13] Duquette J, Rowe A, Wild P. Thermal performance of a steady state physical pipe model for

simulating district heating grids with variable flow. Appl Energy 2016;178:383–93. https://doi.org/10.1016/j.apenergy.2016.06.092.

[14] Chen Y, Wang J, Lund PD. Sustainability evaluation and sensitivity analysis of district heating systems coupled to geothermal and solar resources. Energy Convers Manag 2020;220:113084. https://doi.org/10.1016/J.ENCONMAN.2020.113084.

[15] Vivian J, Emmi G, Zarrella A, Jobard X, Pietruschka D, De Carli M. Evaluating the cost of heat for end users in ultra low temperature district heating networks with booster heat pumps. Energy 2018;153:788–800. https://doi.org/10.1016/j.energy.2018.04.081.

[16] Ommen T, Thorsen JE, Brix Markussen W, Elmegaard B. Performance of ultra low temperature district heating systems with utility plant and booster heat pumps 2017. https://doi.org/10.1016/j.energy.2017.05.165.

[17] Behzadi A, Arabkoohsar A. Comparative performance assessment of a novel cogeneration solar-driven building energy system integrating with various district heating designs. Energy Convers Manag 2020;220:113101. https://doi.org/10.1016/j.enconman.2020.113101.

[18] Pardo García N, Zubi G, Pasaoglu G, Dufo-López R. Photovoltaic thermal hybrid solar collector and district heating configurations for a Central European multi-family house. Energy Convers Manag 2017;148:915–24. https://doi.org/10.1016/j.enconman.2017.05.065.

[19] Rosato A, Ciervo A, Ciampi G, Sibilio S. Effects of solar field design on the energy, environmental and economic performance of a solar district heating network serving Italian residential and school buildings. Renew Energy 2019;143:596–610. https://doi.org/10.1016/j.renene.2019.04.151.

[20] Pakere I, Lauka D, Blumberga D. Solar power and heat production via photovoltaic thermal panels for district heating and industrial plant. Energy 2018;154:424–32. https://doi.org/10.1016/j.energy.2018.04.138.

[21] Emmi G, Bordignon S, Zarrella A, De Carli M. A dynamic analysis of a SAGSHP system coupled to solar thermal collectors and photovoltaic-thermal panels under different climate conditions. Energy Convers Manag 2020;213:112851. https://doi.org/10.1016/j.enconman.2020.112851.

[22] Klein SA et al. TRNSYS 18: A Transient System Simulation Program. 2017; Solar Energy Laboratory, University of Wisconsin, Madison, USA, http://sel.me.wisc.edu/trnsys

[23] ISO 18523-2:2018(en), Energy performance of buildings — Schedule and condition of building, zone and space usage for energy calculation — Part 2: Residential buildings n.d. https://www.iso.org/obp/ui/#iso:std:iso:18523:-2:ed-1:v1:en (accessed April 29, 2021).

[24] ISO 7730:2005(en), Ergonomics of the thermal environment — Analytical determination and interpretation of thermal comfort using calculation of the PMV and PPD indices and local thermal comfort criteria n.d. https://www.iso.org/obp/ui/#iso:std:iso:7730:ed-3:v1:en (accessed April 29, 2021).

[25] Jordan U, Vajen K. DHWcalc: Program to generate domestic hot water profiles with statistical means for user defines conditions. Proc. ISES Solar World Congress, Orlando (US). 2005.

[26] Bordignon S, Emmi G, Zarrella A, De Carli M. Energy analysis of different configurations for a reversible ground source heat pump using a new flexible TRNSYS Type. Appl Therm Eng 2021;197:117413. https://doi.org/10.1016/J.APPLTHERMALENG.2021.117413.

[27] Zarrella A, Emmi G, Vivian J, Croci L, Besagni G. The validation of a novel lumped parameter model for photovoltaic thermal hybrid solar collectors: a new TRNSYS type. Energy Convers Manag 2019;188:414–28. https://doi.org/10.1016/j.enconman.2019.03.030.

[28] EN 12975-2:2006 - Thermal solar systems and components - Solar collectors - Part 2: Test methods n.d. https://standards.iteh.ai/catalog/standards/cen/3ae62ba7-404b-4c89-852d-2124d280eb40/en-12975-2-2006 (accessed December 20, 2021).

[29] Patankar S., Spalding D. A calculation procedure for heat, mass and momentum transfer in three-dimensional parabolic flows. Int J Heat Mass Transf 1972;15:1787–806. https://doi.org/10.1016/0017-9310(72)90054-3.

[30] Vivian J, Quaggiotto D, Zarrella A. Increasing the energy flexibility of existing district heating networks through flow rate variations. Appl Energy 2020;275:115411. https://doi.org/10.1016/j.apenergy.2020.115411.

[31] ASHRAE. 2011. “ASHRAE handbook: HVAC applications, Geothermal Energy”, Atlanta, GA, US, 2011. Chapter 34.

[32] Sartori I, Napolitano A, Voss K. Net zero energy buildings: A consistent definition framework. Energy Build 2012;48:220–32. https://doi.org/10.1016/j.enbuild.2012.01.032.

[33] Note From The French Authorities Subject: Implementation of Directive 2012/27/EU on energy efficiency-Communication from the French authorities of their Annual Report (Article

24 of the Directive).